Palatal Biomechanics and Its Significance for Cranial Kinesis in *Tyrannosaurus rex*

IAN N. COST [1]*, KEVIN M. MIDDLETON,[1] KALEB C. SELLERS,[1] MICHAEL SCOTT ECHOLS,[2] LAWRENCE M. WITMER,[3] JULIAN L. DAVIS,[4] AND CASEY M. HOLLIDAY [1]

[1]Department of Pathology and Anatomical Sciences, University of Missouri, Columbia, Missouri

[2]Echols Veterinary Services, Salt Lake City, Utah

[3]Department of Biomedical Sciences, Heritage College of Osteopathic Medicine, Ohio University, Athens, Ohio

[4]Department of Engineering, University of Southern Indiana, Evansville, Indiana

ABSTRACT

The extinct nonavian dinosaur *Tyrannosaurus rex*, considered one of the hardest biting animals ever, is often hypothesized to have exhibited cranial kinesis, or, mobility of cranial joints relative to the braincase. Cranial kinesis in *T. rex* is a biomechanical paradox in that forcefully biting tetrapods usually possess rigid skulls instead of skulls with movable joints. We tested the biomechanical performance of a tyrannosaur skull using a series of static positions mimicking possible excursions of the palate to evaluate Postural Kinetic Competency in *Tyrannosaurus*. A functional extant phylogenetic bracket was employed using taxa, which exhibit measurable palatal excursions: *Psittacus erithacus* (fore–aft movement) and *Gekko gecko* (mediolateral movement). Static finite element models of *Psittacus*, *Gekko*, and *Tyrannosaurus* were constructed and tested with different palatal postures using anatomically informed material properties, loaded with muscle forces derived from dissection, phylogenetic bracketing, and a sensitivity analysis of muscle architecture and tested in orthal biting simulations using element strain as a proxy for model performance. Extant species models showed lower strains in naturally occurring postures compared to alternatives. We found that fore–aft and neutral models of *Tyrannosaurus* experienced lower overall strains than mediolaterally shifted models. Protractor muscles dampened palatal strains, while occipital constraints increased strains about palatocranial joints compared to jaw joint

This article includes AR WOW Videos. Videos 1–6 can be viewed at https://players.brightcove.net/656326989001/mrOxISgynX_default/index.html?videoId=6058428214001. Videos 7–12 can be viewed at https://players.brightcove.net/656326989001/mrOxISgynX_default/index.html?videoId=6058434297001. Videos 13–18 can be viewed at https://players.brightcove.net/656326989001/mrOxISgynX_default/index.html?videoId=6058438903001.

Abbreviations: FAM = fore–aft movement; FEA = finite element analysis; FEM = finite element model; F_M = muscle force; l_f = fiber length; mAMEM = m. adductor mandibulae externus medialis; mAMEP = m. adductor mandibulae externus profundus; mAMES = m. adductor mandibulae externus superficialis; mAMP = m. adductor mandibulae posterior; mDM = m. depressor mandibulae; mEM = m. ethmomandibularis; MLM = mediolateral movement; mLPT = m. levator pterygoideus; mPM = m. pseudomasseter; mPPT = m. protractor pterygoideus; mPSTp = m. pseudotemporalis profundus; mPSTs = m. pseudotemporalis superficialis; mPTd = m. pterygoideus dorsalis; mPTv = m. pterygoideus ventralis; PCSA = physiological cross-sectional area; PKC = postural kinetic competency; V_M = muscle volume; θ = pennation angle; με = microstrain

Grant sponsor: Division of Earth Sciences; Grant number: EAR-163753; Grant sponsor: Division of Integrative Organismal Systems; Grant numbers: IBN-0407735, IBN-9601174, IOB-0343744, IOB-0517257, IOS 1457319, IOS-1050154, IOS-1456503, IOS-1457319.

*Correspondence to: Ian N. Cost, Department of Pathology and Anatomical Sciences, University of Missouri, Columbia, MO E-mail: incost@mail.missouri.edu

Received 26 June 2018; Revised 13 April 2019; Accepted 22 April 2019.

DOI: 10.1002/ar.24219

Published online 00 Month 2019 in Wiley Online Library (wileyonlinelibrary.com).

constraints. These loading behaviors suggest that even small excursions can strain elements beyond structural failure. Thus, these postural tests of kinesis, along with the robusticity of other cranial features, suggest that the skull of *Tyrannosaurus* was functionally akinetic. Anat Rec, 00:000–000, 2019. © 2019 Wiley Periodicals, Inc.

Key words: cranial kinesis; jaw muscles; skull; *Tyrannosaurus*; bird; lizard; finite element model

Vertebrate feeding adaptations resulted in a diversity of cranial structures and functions, many of which led to changes in palatal functional morphology. Despite these modifications, many reptiles maintain a series of linkages between the palate and braincase that often permit cranial kinesis. Cranial kinesis manifests as a spectrum of palatal motions among lineages (Versluys, 1910; Bock, 1964, 1999; Zusi, 1984, 1993; Gussekloo, 2000; Holliday and Witmer, 2007). Because many of the joints linking the palate to the braincase remain unfused, the skulls of many extinct species of dinosaurs, crocodylomorphs, and other fossil reptiles have also been hypothesized to have had various forms of cranial kinesis (Rayfield, 2005a; Holliday and Witmer, 2007). For example, *Tyrannosaurus rex*, which has plesiomorphic, ball and socket-shaped palatobasal and otic joints, has been hypothesized by different authors to have possessed one of several forms of cranial kinesis (Molnar, 1998; Rayfield, 2004; Larsson, 2008). A functional paradox remains: why do mature individuals of one of the world's most forceful biting, osteophagus animals (Gignac and Erickson, 2017) ever known maintain flexible joints when the hardest biting taxa of other terrestrial lineages (e.g., crocodile, tiger, and hyena; Erickson et al., 2003; Wroe et al., 2005; Tseng and Binder, 2010) suture their cranial elements to form rigid skulls?

Kinetic competency of *Tyrannosaurus* has been explored previously and interpretations and methods vary. Osborn (1912) first remarked on the seemingly mobile nature of particular condylar joints but suggested the surrounding bones limited any particular movement. Also citing the condylar otic joint between the quadrate and squamosal, Molnar (1991, 1998) instead inferred limited streptostyly (rotation of the quadrate about the otic joint) in *Tyrannosaurus*. Rayfield (2004), 2005a, b) inferred numerous sutural and condylar joints within the palate and face of *Allosaurus*, *Tyrannosaurus*, and other theropods to be capable of movement following finite element analysis (FEA) of patterns of stresses. Larsson (2008) extended discussion of *Tyrannosaurus* kinesis and streptostyly with new details on the condylar nature of the palatobasal joint. Conversely, Holliday and Witmer (2007) described *Tyrannosaurus* and many nonavian dinosaurs as being partially kinetically competent, meaning that these taxa possess patent otic and palatobasal joints as well as protractor musculature necessary to mediate powered (driven by muscle force rather than being passive) kinesis. However, these taxa lack permissive linkages in the skull that would enable gross movements of the palate or face. Regardless, these hypotheses have yet to be fully tested in a phylogenetic functional context using 3D modeling techniques.

Permissive linkages in lizards and birds result from the elimination of bones comprising the postorbital and temporal bars, development of craniofacial hinge joints (flexion zones), and the elimination of the epipterygoid in birds. These morphological changes manifest differently in these two clades. Species of lizards exhibit a diversity of often coupled kinetic behaviors including, but not limited to streptostyly, mediolateral motion (MLM) at the palatobasal joint, and mesokinesis (flexion of the facial skeleton about the frontoparietal joint; Rieppel, 1978; Smith and Hylander, 1985; Herrel et al., 2000; Metzger, 2002, Evans, 2003). Many species of birds, including ducks, parrots, and many neoavians also employ streptostyly and prokinesis (elevation of the beak at the craniofacial hinge) as well as concomitant fore–aft motion (FAM) about the palatobasal joint (Hofer, 1950; Burton, 1974a, 1974b; Hoese and Westneat, 1996; Bout and Zweers, 2001; Dawson et al., 2011). Although the palatobasal joint and likely other palatocranial joints are unsutured, they lack mobility in many species of lepidosaurs (Metzger, 2002; Curtis et al., 2010; Jones et al., 2011), birds (Zusi, 1993; Gussekloo, 2005), and nonavian dinosaurs (Holliday and Witmer, 2007).

We use two species of extant, kinetically competent reptiles, tokay geckos (*Gekko gecko*), and grey parrots (*Psittacus erithacus*), to model, frame, and test hypotheses of function in the extinct reptile species *T. rex*. Tokay geckos eliminated the upper and lower temporal bars of their skulls, have large jaw muscles relative to their body size, strut-like pterygoid and epipterygoid bones, and palates connected to the braincase through synchondrodial (cartilaginous without a synovial cavity) otic and diarthrodial (cartilaginous with a synovial cavity) palatobasal joints (Rieppel, 1984; Herrel et al., 2007; Payne et al., 2011; Mezzasalma et al., 2014; Daza et al., 2015). Herrel et al. (1999, 2000) and Montuelle and Williams (2015) found *Gekko* to exhibit a combination of mediolateral and fore–aft streptostyly, long axis rotation of the palate, and bending of the palate about hypokinetic (palatine-pterygoid suture) joints and the mesokinetic hinge. Because the long axis rotation of the palate requires it to also swing mediolaterally, we modeled the palate accordingly in a mediolateral movement, as internal palatal element kinematics remains undescribed.

Grey parrots lack upper temporal bars and epipterygoids, have strut-like lower temporal bars, pterygoids, and quadrates, and articulate the palate to the braincase via diarthrodial otic and analogous "palatobasal" joints between the palate and parasphenoid rostrum (Bailleul and Holliday, unpublished data). Parrots employ prokinesis (Zusi, 1967) in which FAM of the palate occurs at the otic and palatobasal joints to elevate the beak about the craniofacial hinge. These movements are facilitated by large protractor and adductor muscles (Hofer, 1949, 1950), including the neomorphic psittacid pseudomasseter and ethmomandibularis muscles (Tokita, 2003, 2004; Carril et al., 2015).

Given previous research (Molnar, 1991, 1998; Carr, 1999; Rayfield, 2004, 2005a; Snively et al., 2006; Molnar, 2008; Holliday, 2009; Bates and Falkingham, 2012; Gignac and Erickson, 2017), we know enough about *Tyrannosaurus* cranial anatomy to rigorously explore hypotheses of cranial behavior and function and examine the kinetic capacity of these forcefully biting ancient predators. The skulls of *Tyrannosaurus* and many other nonavian theropod dinosaurs maintain both upper and lower temporal bars, epipterygoids, dorsoventrally thin palatal elements, and robust scarf joints between elements of the dermatocranium and palate (Molnar, 1991, 1998; Carr, 1999; Snively et al., 2006), all of which are features considered to limit cranial mobility (Holliday and Witmer, 2007). Regardless, Molnar (1991), Rayfield (2005a), and Larsson (2008) hypothesized FAM via streptostyly in *Tyrannosaurus* based on the ball and socket-shaped (i.e., condylar) otic and palatobasal joints. These joints are spanned by large adductor muscles laterally (Molnar, 2008; Holliday, 2009; Bates and Falkingham, 2012; Gignac and Erickson, 2017) as well as large, tendinous protractor muscles medially (Holliday and Witmer, 2007; Holliday, 2009). Here we test the performance of *Tyrannosaurus* finite element models (FEMs) compared to those of known, kinetically competent *Gekko* and *Psittacus* models. Accurately modeled jaw muscle loads and joint articulations were integrated into each model in akinetic (neutral), MLM (MLM of the palate about the otic and palatobasal joints), and FAM (FAM about the otic and palatobasal joints postures). Strains of the models were analyzed qualitatively and quantitatively to determine the optimal and most likely posture of the *Tyrannosaurus* palate. A better understanding of the loading environment of the skull and kinetic competency of extinct dinosaur species like *T. rex* illuminates vertebrate adaptations for feeding, the evolutionary development of cranial joints, and the origins of avian-style cranial kinesis from nonavian theropod dinosaurs.

METHODS

Finite element modeling is a common approach used to evaluate biomechanical performance of dinosaur skulls (Rayfield, 2004; Moazen et al., 2009; Lautenschlager et al., 2013; Lautenschlager, 2015). Although many studies employ models of taxa for specific instances of feeding behaviors, few explore changes in gape and other excursions of cranial elements during feeding cycles (e.g., Moazen et al., 2008; Lautenschlager, 2015). Similarly, here we test the performance of several different kinetic postures across a sample of taxa. The heads of *P. erithacus* (MUVC AV042) and *G. gecko* (MUVC LI044) were scanned in a Siemens INVEON SPECT/CT (VA Biomolecular Imaging Center, Columbia, MO) with voxel sizes of 63.4 and 92.1 μm, respectively. A 1/6-scale model of *T. rex* (BHI 3033) was scanned in a General Electric LightSpeed Ultra Multislice CT scanner (voxel size of 625 μm, 120 kV, 170 mA, OhioHealth O'Bleness Memorial Hospital, Athens, OH). CT data were segmented in Avizo Lite 9 (FEI Company, Hillsboro, OR).

Bones of the palate and the rostrum (in *Gekko* and *Psittacus*) were segmented separately from bones of the neurocranium and dermatocranium in each model, allowing for postures to be modified (See Table 1 for segmented elements). Stereolithographical models (STL files) were generated from segmentation and were cleaned and repositioned in anatomical postures of hypothesized kinesis in Geomagic (3D Systems, Rock Hills, SC). Skeletal elements were joined together prior to construction as FEMs. FEMs were constructed in Strand7 (Strand7 Pty. Ltd., Sydney, Australia) using four point tetrahedral elements. Joints between the palate and braincase, and kinetic hinges in *Gekko* and *Psittacus*, were then broken to simulate mobile joints. Connections between the now open elements were linked to one another with beams assigned the properties of joint materials. Beam number within the joint areas was dependent on the size of the articular surfaces of bones forming the joints.

Postural kinetic competency (PKC) models were constructed using the BoneLoad workflow (Grosse et al., 2007; Davis et al., 2010; Sellers et al., 2017, Fig. 1). BoneLoad distributes the estimated muscle forces in each postural model across the attachment sites of muscles which are in turn used to load the model. Joint materials were modeled using links and beams to emulate different articular tissue material properties (e.g., suture/ligament, hyaline cartage, bone). This approach differs from other models that included ligamentous connections modeled as continuous layers of brick elements with different material properties to emulate cranial sutures (Moazen et al., 2009; Reed et al., 2011; Curtis et al., 2013; Jones et al., 2017). In general, the models built here using linkages are more yielding than previous models. Greater flexibility in our modeled joints should allow for better dissipation of forces in biologically accurate biomechanical environments than fully fused FEMs (e.g., Moazen et al., 2009; Jones et al., 2011).

Models were built in three positions, which approximate different kinetic motions: akinesis (hereafter referred to as the neutral posture), FAM, and MLM. Each model was constructed to exhibit a neutral posture by opening the mandible to a 20-degrees gape without shifting either the quadrate or palate. A posture resulting from FAM (prokinesis

TABLE 1. Segmented skeletal elements, constructed joints, and mobile elements represented in each taxon in this study

Taxon	Elements segmented	Joints modeled	Mobile elements in final model
Gekko	Palatine, pterygoid, rostrum, quadrate, mandible, neuro/dermatocranium	Palatobasal, otic, frontoparietal hinge	Rostrum, palatine, pterygoid, epipterygoid, quadrate
Tyrannosaurus	Palatine, pterygoid, rostrum, epipterygoid, ectopterygoid, vomer, quadrate, mandible, neuro/dermatocranium	Palatobasal, otic	Pterygoid, epipterygoid, ectopterygoid, quadrate
Psittacus	Palatine, pterygoid, jugal, rostrum, quadrate, mandible, neuro/dermatocranium	Palatobasal, otic, craniofacial hinge	Rostrum, palatine, pterygoid, quadrate, jugal

Mobile elements are defined as elements of the palate that are capable of moving as a result of being joined to the cranium by joint and sutural materials only in the finite element model. These entities are consistent across postures within each taxon.

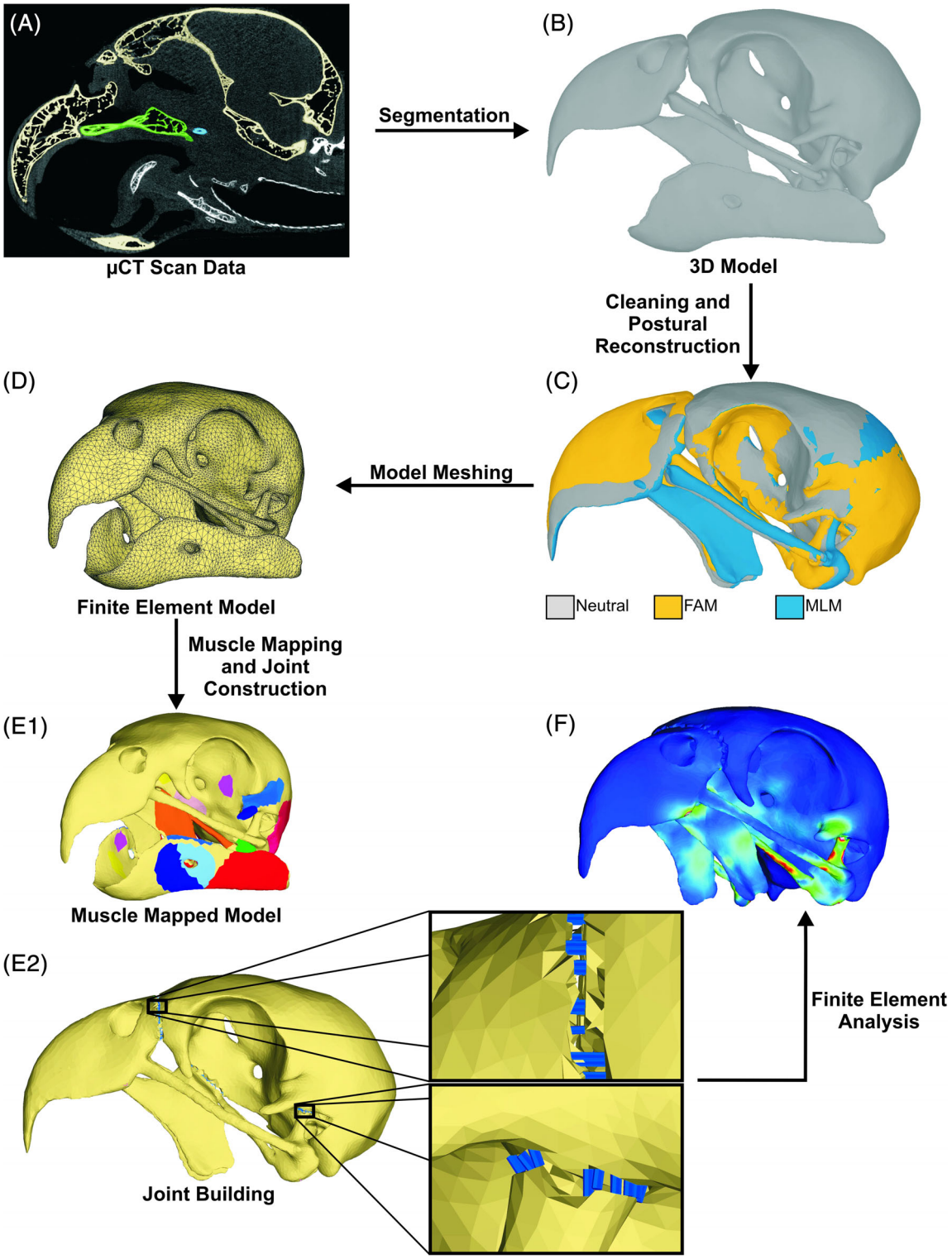

Fig. 1. Postural Kinetic Competency modeling workflow followed in this study. Microcomputed Tomography data (**A**) are segmented to build 3D models by segmenting individual bones (or bony segments; e.g., beak, braincase) as separate elements (**B**). 3D models are reconstructed in kinetic postures with individual elements realistically articulated (**C**). The resulting models are imported into Strand7 as stereolithographical files and are meshed using 4-node tetrahedra (**D**). Meshed models are prepared for finite element analysis (FEA) by mapping muscles on the surface and eliminating tetrahedra in joint areas (**E1**). Beams are attached to the facing sides of joint surfaces and are given material properties reflecting capsular or sutural ligaments (**E2**). The resulting finite element model is loaded using distributed muscle forces via the BoneLoad MATLAB program and Strand7 FEA software (**F**).

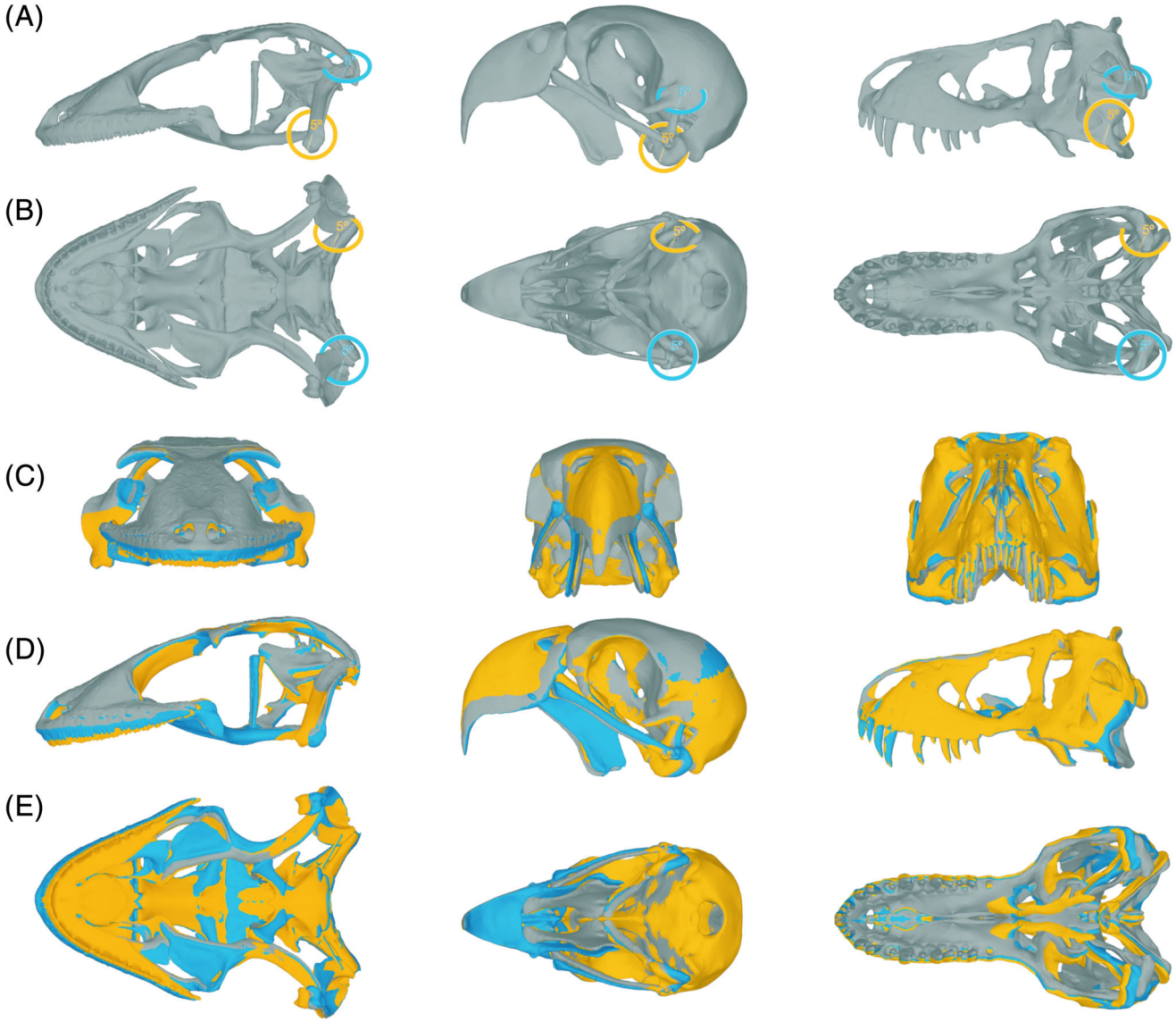

Fig. 2. Comparisons of postures using overlays of each of the three models: Left, *Gekko gecko*; Middle, *Tyrannosaurus rex*; Right, *Psittacus erithacus* showing postural change in left lateral (**A**) and ventral (**B**) views and in rostral (**C**), lateral, (**D**), and ventral (**E**) views showing overlaid postural configurations used to model kinetic competency. Postures are overlaid using the jaw joint as the origin of the axes. Neutral models are represented in gray, FAM models in orange, and MLM models in blue. Angles of rotation/translation at the otic joint are shown using color-coded angle measurements in (A) and (B).

+ streptostyly), and a posture resulting from MLM (streptostyly + hypokinesis + mesokinesis) created by initially shifting the quadrate at the otic joint 5-degrees rostrocaudally and 5-degrees medially (Fig. 2). Previous studies detected quadrate rotations between 5 and 10-degrees in extant taxa (Hoese and Westneat, 1996; Herrel et al., 1999; Metzger, 2002; Montuelle and Williams, 2015; Claes et al., 2016). A movement of 5-degrees, therefore, is a conservative estimate of streptostylic quadrate movement.

To model soft-tissue attachment sites, models were imported to Strand7 and material properties assigned to specific regions of the models. All models were assigned isotropic materials during construction and identical bone properties (E = 13.65 GPa *sensu* Rayfield, 2011; ν = 0.3). Articulated palatobasal and otic joints, the frontoparietal joint, and the craniofacial hinge were built by eliminating bricks in the joint space and linking portions of the model to one another using structural beams attached to the facing sides of the joints. Other potentially mobile joints, such as the epipterygoid-pterygoid in the gecko, or the quadrate-quadratojugal joint and palatine-maxillary joint in the parrot, were left fused to focus on strains at primary locations of kinesis in the palate and quadrate. Joints were reconstructed in *Psittacus* and *Gekko* using beam properties simulating rat cranial sutures (E = 2.35 MPa, ν = 0.3; Chien et al., 2008). *Tyrannosaurus* joints were reconstructed using beam properties simulating canine patellar tendon (E = 4.57 MPa, ν = 0.3; Haut et al., 1992). Joint materials of different-sized animals were used in an attempt to mimic joints of closer physiological size in the taxa of interest. Sensitivity analysis

was conducted using the sutural materials of the *Tyrannosaurus* model in *Psittacus* to determine the role these values may have played in the analysis.

Muscle attachment sites were mapped onto models using information from dissection, observation, and the literature (Hofer, 1950; Abdala and Moro, 1996; Herrel et al., 1999;

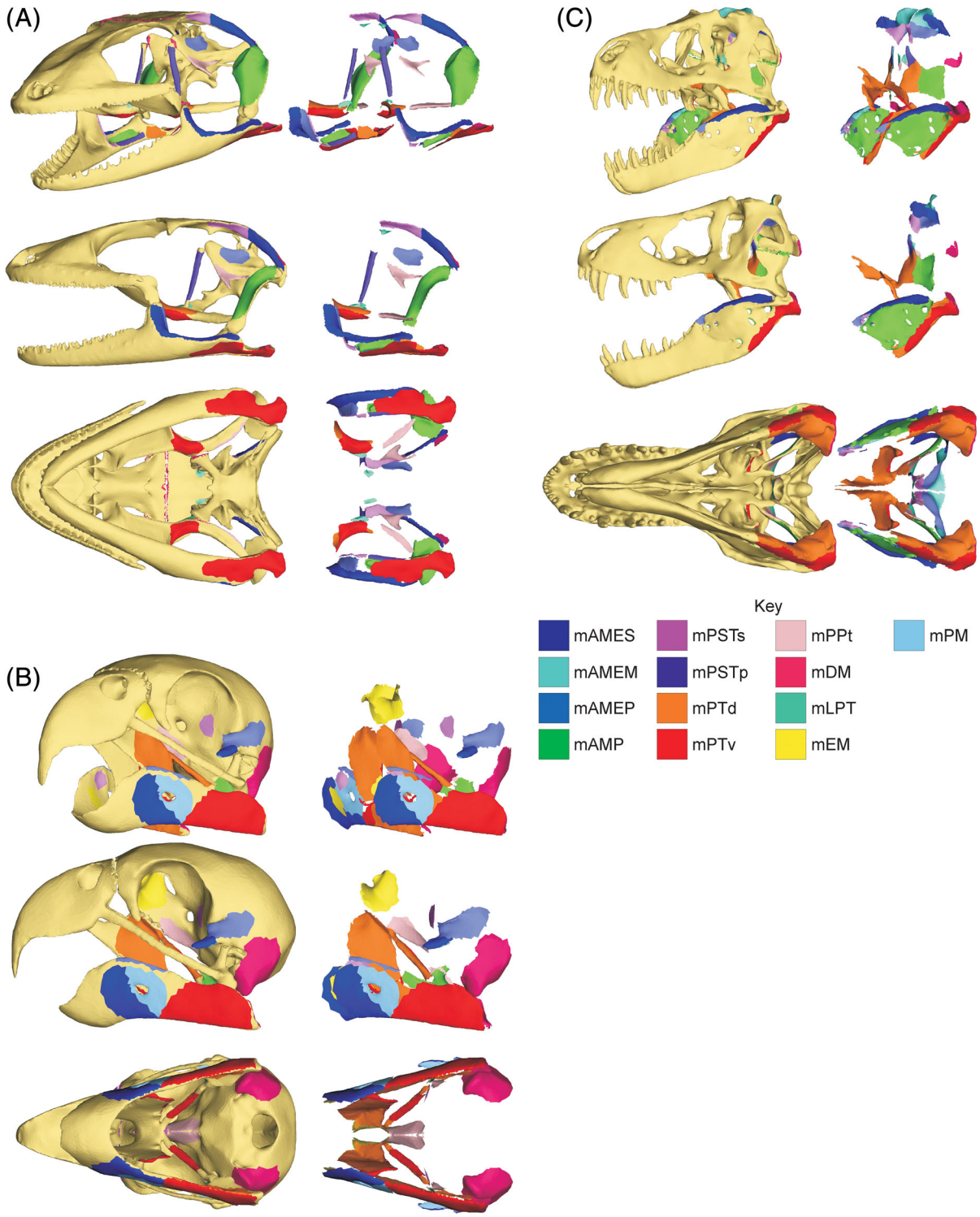

Fig. 3. Mapped attachments of jaw muscles used to load finite element models of (**A**) *Gekko gecko*; (**B**) *Psittacus erithacus*, and (**C**) *Tyrannosaurus rex* in Top: left oblique; Middle: left lateral; and Bottom: ventral views for each taxon. Muscle map colors follow same palate and hypotheses of homology as Holliday (2009).

Tokita, 2004; Holliday, 2009; Carril et al., 2015; Fig. 3). Anatomical details for muscle fiber length and pennation of fibers relative to central axes were measured in *Gekko* and *Psittacus* and compared to the literature (e.g., Herrel et al., 1999; Hieronymus, 2006; Carril et al., 2015; Table 2) to estimate physiological cross-sectional area (PCSA) using equation (1) (Sacks and Roy, 1982):

$$\mathrm{PCSA} = \frac{V\mathrm{M}}{l\mathrm{f}} \times \cos(\theta), \quad (1)$$

where V_M is the muscle volume, l_f is the fiber length, and θ is the pennation angle of the muscle.

The pennation angles of *Tyrannosaurus* jaw muscles were estimated to fall within known pennation angles of alligator, bird, and lizard jaw muscles based on visible osteological correlates suggestive of tendon attachments as well as coarse phylogenetic bracketing. Hence, muscles with pennate extant homologs and informative osteological correlates were conservatively modeled as more pennate than other muscles. For example, m. adductor mandibulae externus profundus, which is the large muscle that attaches to the dorsotemporal fossa and is relatively pennate in most vertebrates, was modeled with 20-degrees pennation angle, whereas m. adductor mandibulae posterior, which attaches to the body of the quadrate, was modeled as being largely parallel fibered (5-degrees pennation angle) given the lack of clear tendinous scars on the quadrate in *Tyrannosaurus* and its relatively simple architecture in birds, non-crocodyliform suchians (Holliday and Witmer, 2009), and archosaur outgroups (e.g., lizards; Haas, 1973; Holliday and Witmer, 2007; Holliday, 2009). All muscles were modeled to have fiber lengths that were two-third the length of the muscle itself, which is also generally conservative across vertebrates (Bates and Falkingham, 2018).

To further justify our phylogenetically bracketed estimates of jaw muscle architecture in *Tyrannosaurus*, we developed a sensitivity analysis to explore the effects of fiber length and pennation on PCSA. Because fiber length and pennation angle are the physiological parameters that modulate the force predicted from anatomical cross-sectional area for a given muscular geometry, PCSA and, by extension, muscle force is a function of fiber length and pennation alone. In theory, pennation can vary from 0-degrees asymptotically to 90-degrees, and fiber length can vary from 1 asymptotically to 0. To explore the parameter space of pennation and fiber length, we calculated the PCSA of each jaw muscle of *Tyrannosaurus* for 100 values of pennation ranging from 0 to 89.1-degrees and 100 values of fiber length ranging from 0.01 to 1, for a total of 10,000 combinations per muscle. This range captures the full potential range of the factors that contribute to PCSA in *Tyrannosaurus*.

Muscle volume, fiber architecture (Table 2), and muscle attachment centroids were then used to calculate 3D resultants of jaw muscles as well as ultimately distributed loads on the FEM *sensu* Sellers et al. (2017) using equation (2):

$$F\mathrm{M} = \mathrm{PCSA} \times T\mathrm{specific}, \quad (2)$$

where $T_{specific}$ is specific tension (Porro et al., 2011), and F_M is muscle force. The resultant muscle force and muscle attachment centroids serve as muscle parameter input in the BoneLoad workflow. Models were all constrained at bilateral, caudal bite points. All models are constrained by single nodes at the mandibular condyle of the quadrate in

TABLE 2. Muscle parameters used to estimate physiological cross-sectional areas and jaw muscle force used in finite element models

		mAMES	mAMEM	mAMEP	mAMP	mPSTs	mPSTp	mPTd	mPTv	mPPT	mEM	mPM	mLPT	mDM
Fiber length (cm)	*Gekko*	1.3		1.1	0.8	1.3	0.8	0.8	0.8	0.4			0.8	1
	T. rex	46	52	57	28	55	41	32	28	10			6	25
	Psittacus	1.6		1.5	0.3	1.4		1.2	1.0	1.0	1.6	2.1		0.7
Pennation angle (θ)	*Gekko*	20		0	5	0	0	15	15	5			5	5
	T. rex	0	0	0	15	10	10	10	15	15			0	5
	Psittacus	20		20	0	6.66		14.54	4.09	0	2.57	0		5.52
Muscle volume (cm^3)	*Gekko*	0.445		0.180	0.463	0.141	0.128	0.093	0.391	0.072			0.028	0.066
	T. rex	20,971	17,729	11,914	37,120	7,792	2,668	40,106	8,562	2,187			545	8,981
	Psittacus	1.07		0.070	0.006	0.026		2.63	1.54	0.036	0.098	1.24		0.084
Force (N)	*Gekko*	9.25		4.58	16.84	3.11	4.28	3.44	13.77	4.49			1.12	1.96
	T. rex	3,343	9,841	6,635	39,859	4,209	1,865	34,816	8,820	5,489			3,180	10,206
	Psittacus	21.17		13.41	6.90	6.20		63.11	47.38	11.38	19.99	17.59		35.37

Abbreviations: mAMES, m. adductor mandibulae externus superficialis; mAMEM, m. adductor mandibulae externus medialis; mAMEP, m. adductor mandibulae externus profundus; mAMP, m. adductor mandibulae posterior; mDM, m. depressor mandibulae; mEM, m. ethmomandibularis; mPM, m. pseudomasseter; mPSTs, m. pseudotemporalis superficialis; mPSTp, m. pseudotemporalis profundus; mPTd, m. pterygoideus dorsalis; mPTv, m. pterygoideus ventralis; mPPT, m. protractor pterygoideus; mLPT, m. levator pterygoideus.

all planes of movement and at a series of occipital attachments near the approximate center of muscle attachments, *sensu* Snively and Russell (2007). Muscles were activated simultaneously at maximal force in each model similar to the methods used by Bates and Falkingham (2012) to estimate the bite force of *Tyrannosaurus*. Muscle activation patterns were also addressed during *post hoc* testing. Strain data were analyzed across the cranium and within skeletal elements to describe kinetic competency and the likelihood of kinetic postures in the analyzed taxa. Tetrahedral ("brick") strains were sampled in specific regions of the skeletal elements of the palate. Surface tetrahedrals in regions of interest were selected as pools to sample from which included anterior, middle, and caudal portions of the palatine and pterygoid bones. The quadrate was sampled in otic, middle, and ventral regions because this bone is oriented perpendicularly to the palatine and pterygoid bones. The regions were then subsampled randomly using a random number generator (built in Microsoft Excel) to assign 50 rows of data to be included in the quantitative analyses.

We expected neutral posture models to exhibit a base level of strain in the palatal elements. Postural kinetic competencies exhibiting strain in the palates higher than the neutral posture models represent less likely loading conditions. Conversely, models exhibiting strain in the palates lower than the neutral PKCs were considered acceptable, more likely, anatomical configurations. Although the local effects of strain on bone tissue growth and resorption are complicated (e.g., Frost, 1987; Martin, 2000; Herring and Ochareon, 2005), Curtis et al. (2011), using FEA for bone strain, as we are here, hypothesized that cranial elements in *Sphenodon* and other vertebrates assumed shapes that were best adapted to their average loading environments as a means of optimizing strain across the entire skull. Thus, although higher and lower strains are not fundamentally "bad" or "good," we can expect behaviors such as joint excursions that elicit exceptionally higher strains in elements to be less optimal than other behaviors. We define structural failure in our models as strains that exceed 6,000 microstrain (με) because this value is contained within ranges of the estimated strain of bone failure (e.g., Reilly and Currey, 1999; Campbell et al., 2016).

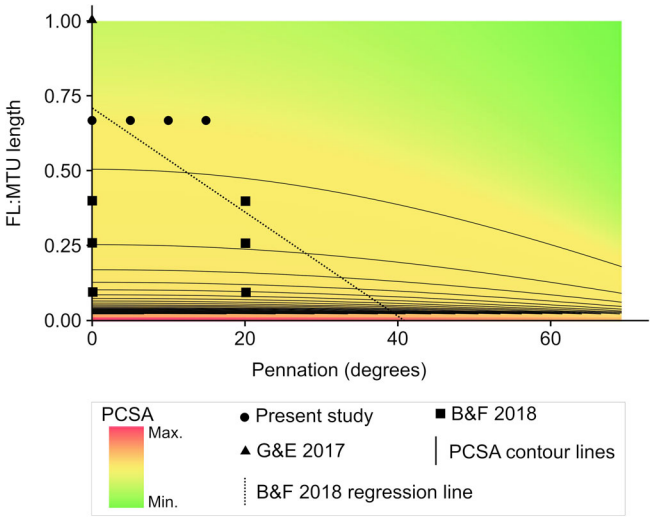

Fig. 4. The relationship between fiber length, pennation angle, and force in muscle physiology and its application to reconstructing function in fossil taxa using recent case studies. PCSA is a function of pennation angle and fiber length and is mapped as a heatmap with contour lines. We replotted the regression line from Bates and Falkingham, 2018 (labeled "B&F 2018") showing the classic prediction that increasing pennation in order to accommodate shorter muscle fibers increases PCSA. PCSA values from recent studies, Gignac and Erickson, 2017 (labeled "G&E 2017") and Bates and Falkingham, 2018, of *Tyrannosaurus* cranial biomechanics are also plotted to show similarities in approaches.

RESULTS

Muscle and Bite Forces in Extant Species

Modeled *Psittacus* bite force (61.78N [rostral bite position]–96.44N [caudal bite position]) was greater than the 16.74N reported for Monk Parakeets (*Myiopsitta monachus*) estimated using PCSA by Carril et al. (2015) as expected given that the skull of *P. erithacus* is about twice as large. Bite forces in our *Gekko* models (11.27N [rostral bite position]–18.53N [caudal bite position]) were near ranges reported by both Anderson et al. (2008; 10.1N–19.1N) and Herrel et al. (2007; 10.78N–16.97N) using bite force meters.

Sensitivity Analysis of Muscle Forces in *Tyrannosaurus*

The distribution of PCSA values of our sensitivity analysis of theoretical muscle architecture is represented using a heatmap (Fig. 4). Although pennation angle and fiber length are the two parameters on which PCSA depends, there is a functional relationship between pennation and fiber length in which fiber length has a stronger effect on PCSA than pennation angle. For example, when we hold fiber length constant (any horizontal line on Fig. 4), larger values of PCSA are associated with low pennation angle, and the largest value was 64 times the smallest value (approximately equal to $\cos^{-1}$ (89.1-degrees)). When we hold pennation angle constant (any vertical line on Fig. 4), larger values of PCSA are associated with shorter fiber length, and the largest value was 100 times larger than the smallest value (equal to 0.01^{-1}). This and the construction of the PCSA equation show that the effect of fiber length is greater than that of pennation angle on PCSA (*sensu* Gans and De Vree, 1987).

Upon this heatmap (Fig. 4), we project the regression line of Bates and Falkingham (2018), which compiled over 1,000 measured vertebrate muscles, along with plots of Bates and Falkingham's (2012), Gignac and Erickson's (2017), and our phylogenetically bracketed *Tyrannosaurus* muscle architecture data. Bates and Falkingham's (2012) muscle force estimates used combinations of pennation angles of 0–20-degrees and fiber lengths of 0.1–0.4 times muscle length (i.e., 1/10–2/5 times muscle length), which resulted in forces below the regression line, thus corresponding to higher forces. Gignac and Erickson (2017) modeled muscles with 0-degrees pennation and a fiber length equal to muscle length, the combination of which yields the lowest possible PCSA. The PCSA estimates in *Tyrannosaurus* from the present study fall close to the regression line of all known vertebrate PCSAs published by Bates and Falkingham (2018), suggesting that the values we used are close to predictions from extant taxa and our bite force estimates are reasonable.

Bite forces in our *Tyrannosaurus* model (35,365N–63,492N) extensively overlap with the range reported by Bates and Falkingham (2012; 18,065N–57,158N) and are about twice the magnitude predicted by Gignac and Erickson (2017; 8,526–34,522N). These differences between our results and those of Gignac and Erickson (2017) are likely due to our inclusion of pennate jaw muscles, whereas the latter authors modeled all jaw muscles as parallel fibered.

Analyses of Strain Patterns

Strain differences were found among the *Gekko* models with respect to the bones, sampling region, and posture. The neutral *Gekko* model (Fig. 5A; Supporting Information Videos 1–6: https://players.brightcove.net/656326989001/mrOxISgynX_default/index.html?videoId=6058428214001) exhibited higher strains in the pterygoid than those in the quadrate or the palatine. The ventral portion of the epipterygoid was extremely strained around the joint with the pterygoid, which may be an artifact of the modeling process wherein the epipterygoid and pterygoid were fused together. The body of the pterygoid, however, is strained across its length, representing a higher strain concentration than in any of the other elements of the palate (Fig. 5A). The FAM *Gekko* model reveals high strains in the quadrate, and pterygoid suggesting that this is not an optimal posture (Fig. 5B). However, the MLM *Gekko* model (Fig. 5C) exhibits low strains in the elements of the palate, suggesting that the MLM model is a more optimal posture, along with the neutral posture. The otic process retains slightly higher strains than the other portions of the quadrate in the MLM model. The pterygoid still possesses localized higher strains (Fig. 5C), though these are lower compared to the pterygoid in the FAM model (Fig. 5B).

The MLM model of *Gekko* (Fig. 6) possessed lower median strain values (1,731 με) than those of neutral (2,277 με) or FAM (2,714 με) postures (Table 3). The lowest strain values of *Gekko* are found in the palatines. However, strains were lowest in different portions of the palatine in each of the postural models of *Gekko*. The ventral portion of the quadrate was most strained in the FAM *Gekko* model (6,322 με) and least strained in the neutral posture (1,767 με). Median strain values of whole elements are shown for all taxa in Table 4. The otic and middle regions of the quadrate possessed identical strain profiles in all three postures, despite differences in rotation at the otic joint. Similarly, the pterygoid exhibited a conserved pattern of caudal to rostral strain decrease across all models. The caudal to rostral pattern is observed in the FAM posture in the palatines; however, this is reversed in the neutral posture. In the MLM posture, the rostral region of the palatine was subjected to more strain than the middle region but the caudal region was subjected to the highest strain.

The *Psittacus* models also experienced differing strains in the bones, sampling region, and between postures. In the neutral *Psittacus* model (Fig. 5D; Supporting Information Videos 7–12: https://players.brightcove.net/6563269 89001/mrOxISgynX_default/index.html?videoId=6058434 297001), the quadrate and pterygoid experienced high strain relative to other parts of the cranium (Fig. 5D). The palatine, postorbital process, and the interorbital septum experienced low strains in this posture despite serving as muscle attachment sites (Fig. 5D). The FAM *Psittacus* model revealed high strains on the rostral aspects of many of the kinetic palatal elements (Fig. 5E). In the MLM *Psittacus* model (Fig. 5F), strains are noticeably higher at the otic process of the quadrate, the postorbital process, and the middle of the palatine compared to the FAM model (Fig. 5D). Strain in the pterygoid is relatively uniform throughout the bone compared to that seen in the palatine.

In *Psittacus* (Fig. 7), the MLM model exhibited higher overall median strain of the palate (753 με) than neutral (619 με) or FAM (543 με) models (Table 3). Strain values of the FAM model were the lowest, as expected by observations of feeding behaviors. The MLM model possessed higher overall strains in the palatine and pterygoid, maintaining the same trend as the other *Psittacus* postures. Pterygoid strains in the MLM model increased from the middle and caudal regions to the rostral region whereas in the neutral model strain steadily decreased moving rostrally. In the FAM model, peak strains were found in the caudal region of the pterygoid, however, the middle region appeared to possess decreased strain. The strain again increased in the rostral sampling region. In all three postures strain decreased from caudal to rostral in the palatines. The otic process of the quadrate possessed the highest strain values across all postural models of *Psittacus*.

Strain differences found among the *Tyrannosaurus* model's bones, sampling regions, and between postures were highlighted by areas of structural failure. The neutral *Tyrannosaurus* model (Fig. 5; Supporting Information Videos 13–18: https://players.brightcove.net/656326989001/mrOxISgynX_default/index.html?videoId=6058438903001) exhibited low strain throughout the palate with the exception of modeling artifacts at joints of the palate. The caudal portion of the pterygoid was weakly strained whereas the body of the quadrate experienced higher strains in the neutral posture (Fig. 5G). The palatine and pterygoid exhibited higher strains across their rostral bodies and the quadrate showed high strain values across pterygoid and otic processes (Fig. 5G). The joints of the FAM *Tyrannosaurus* model (Fig. 5H) were increasingly strained, particularly at isthmuses and articulations with the cranium. Lower overall strain was found throughout the FAM model, but areas of failure remained prevalent across the palate (Fig. 5H). The palatine of the FAM model exhibited lower overall strain than the other elements in the palate (Fig. 5H). The MLM *Tyrannosaurus* model found the otic joint to be highly strained, and the bodies of the quadrate, pterygoid, and palatine bones to all be highly strained (Fig. 5I). High strains also propagated throughout the facial skeleton in the MLM model (Fig. 5I). Failures in the MLM model were observed throughout the pterygoid and the dorsal ridge of the quadrate body (Fig. 5I). Across the *Tyrannosaurus* models, the lower temporal bar experiences high strains near the quadratojugal-jugal suture that approach or exceed levels of structural failure (Fig. 5G–I).

Tyrannosaurus (Fig. 8) exhibited different quantitative strain profiles across the three postural models. The MLM model exhibited the highest median strain values (1,768 με) of the three postural models (neutral 1,542 με; FAM 1259 με; see Table 3). Across all three postures, the quadrate was similarly strained overall, though the middle region was more variable (Fig. 8). The middle region of interest was subjected to more strain than the ventral or otic regions in all postures, but

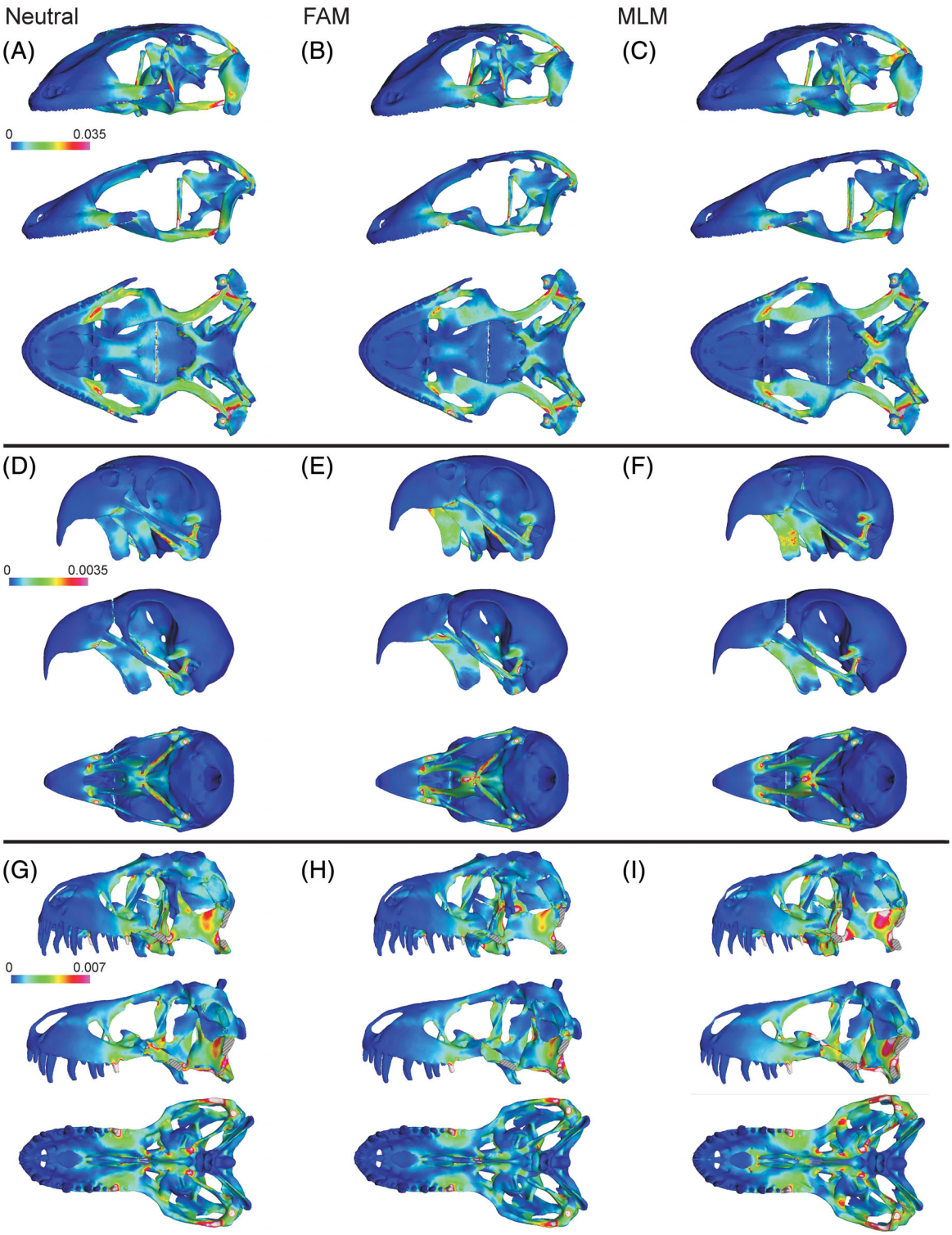

Fig. 5. Heat maps depicting Von Mises strains in *Gekko gecko* (**A–C**), *Psittacus erithacus* (**D–F**), and *Tyrannosaurus rex* (**G–I**) in Left, Neutral; Middle, FAM; and Right, MLM postures of each taxon. Models are shown in left oblique (top), left lateral (middle), and ventral (bottom) views. Heat maps show strains in postural models with all muscles fired simultaneously. Areas of high strain appear in warmer colors; white areas are beyond the scales presented with the models. Cooler colors depict areas of low strain concentration. Bones of the left lateral dermatocranium (i.e., portions of the maxilla, jugal, lacrimal, postorbital, and quadratojugal bones) have been removed on heat maps of *T. rex* to show details of the palate, although all bones were in place for the analysis.

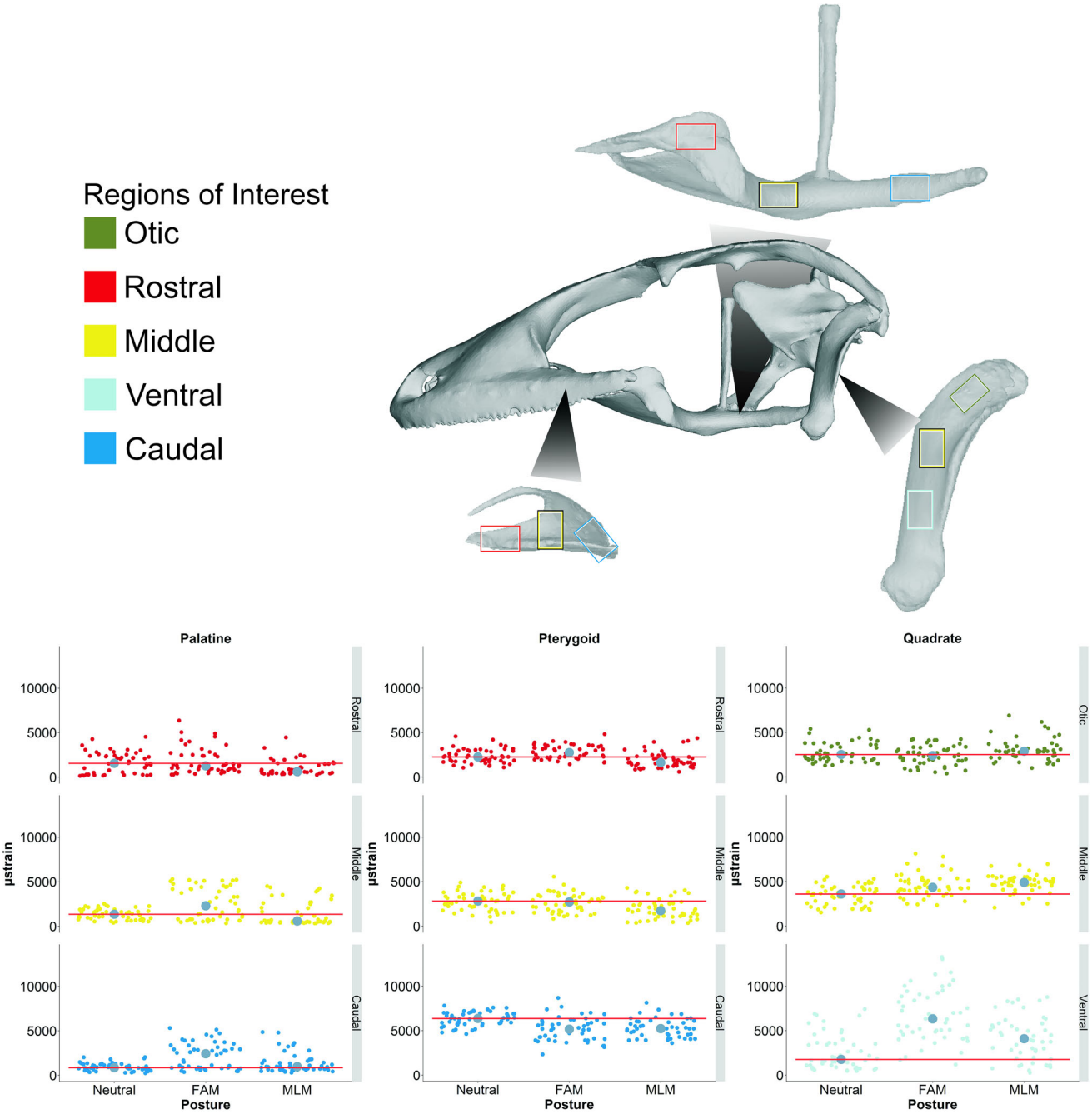

Fig. 6. Strains of regions of interest in the palatal elements of *Gekko gecko*. Regions of interest and scatter plots showing individual sample points as well as median strains (color-coded by sampling region) are represented. Otic, middle, and ventral regions correspond to sampling of the quadrate whereas rostral, middle, and caudal regions correspond to sampling areas of the palatine and pterygoid. Each sampling region consists of 50 tetrahedra sampled randomly from the surface of the skeletal element. Horizontal lines representing the median value of the neutral posture are shown in red in each region of the palatal bones to facilitate comparison across postures.

especially in the MLM posture (Fig. 8). The neutral posture exhibited similar ventral and otic strains (1,540 and 1,459 με, respectively); however, the otic strains were noticeably higher in both the MLM and FAM models (1,980 and 2,029 με, respectively). The pterygoid in the MLM posture of *Tyrannosaurus* was subjected to greater strain than either the neutral or FAM postures. The rostral region of the pterygoid was subjected to the least strain by large margins in both the neutral and MLM models. The most appreciable difference between models, however, can be seen within the caudal portions of the three models (Fig. 8). A slight increase was observed from middle to rostral in the FAM model. In all three postures, the palatine exhibited the highest median strains in the rostral portion with similar strain patterns in the caudal and middle aspects as well. The caudal portion of the palatine was subjected to low

TABLE 3. Median strain of entire palate by model

Taxon	Posture	Median Strain
Gekko gecko	Neutral	2,277.36
	MLM	1,731.44
	FAM	2,714.28
Tyrannosaurus rex	Neutral	1,542.46
	MLM	1,768.37
	FAM	1,259.19
Psittacus erithacus	Neutral	619.13
	MLM	753.24
	FAM	543.55

Quadrate, pterygoid, and palatine regions of interest are taken into account in these medians. Abbreviations: FAM, fore–aft movement; MLM, mediolateral movement.

TABLE 4. Median strain of palate elements organized by posture for each taxon

Taxon	Bone	Posture	Median Strain
Gekko gecko	Palatine	Neutral	1,346.01
	Pterygoid	Neutral	2,822.19
	Quadrate	Neutral	2,516.53
	Palatine	MLM	620.17
	Pterygoid	MLM	1,731.44
	Quadrate	MLM	4,094.59
	Palatine	FAM	2,300.19
	Pterygoid	FAM	2,759.20
	Quadrate	FAM	4,341.22
Tyrannosaurus rex	Palatine	Neutral	995.86
	Pterygoid	Neutral	1,993.55
	Quadrate	Neutral	1,540.88
	Palatine	MLM	1,024.31
	Pterygoid	MLM	2,348.10
	Quadrate	MLM	1,980.55
	Palatine	FAM	534.07
	Pterygoid	FAM	1,259.19
	Quadrate	FAM	2,029.88
Psittacus erithacus	Palatine	Neutral	326.41
	Pterygoid	Neutral	1,121.62
	Quadrate	Neutral	412.29
	Palatine	MLM	753.24
	Pterygoid	MLM	884.82
	Quadrate	MLM	258.73
	Palatine	FAM	455.94
	Pterygoid	FAM	587.26
	Quadrate	FAM	210.53

Multiple regions of interest are taken into account in determining the median values of each bone (quadrate, pterygoid, and palatine). Abbreviations: FAM, fore–aft movement; MLM, mediolateral movement.

median and overall strains in all three models, but this is especially so in the FAM model (Fig. 8).

DISCUSSION

Tyrannosaurus Was Functionally Akinetic

By incorporating cranial joint articular tissues, distributed muscle loads, and posture analysis to infer cranial performance in *T. rex*, we have gained a nuanced understanding of the biomechanics of the skull. We accurately estimated the biomechanical environment of *Gekko* and *Psittacus* using PKC methods and achieved lifelike results prior to modeling *T. rex*. Rotation of the quadrate 5-degrees rostrocaudally and mediolaterally was sufficient to affect the rostral elements of the palate and the facial skeleton such that lifelike fore–aft and MLMs were reflected in the models of both extant taxa. Functionally acceptable ranges of strain were observed in models of FAM in *Psittacus* and MLM in *Gekko*. Equally important, MLM in *Psittacus* and FAM in *Gekko* resulted in failures at joints, within individual bones, and across the palate. Thus, the loading behavior of the *Tyrannosaurus* model also performs with acceptable accuracy with respect to the anatomical potential of the animal. Using these findings, we conclude that *Tyrannosaurus* was functionally akinetic. Although hypotheses of fore–aft palatal motion in *Tyrannosaurus* are more supported compared to those of mediolateral palatal motion, the linkages surrounding the otic joint impede fore–aft excursions of the quadrate, and the loading that the palate and craniofacial skeleton experience during bites suggests powered, fore–aft kinesis is extremely unlikely. Like paleognaths (Gussekloo, 2005), many iguanians and other lepidosaurs (Jones et al., 2017), many dinosaurs (Holliday and Witmer, 2007), stem crocodylomorphs (Pol et al., 2013), and numerous diapsid species, including *Tyrannosaurus*, remain akinetic despite possessing unsutured otic and palatobasal joints.

Cranial kinesis in *Tyrannosaurus* has been debated since shortly after the initial description of the taxon. Osborn (1912) recognized the morphological limitations of kinesis in *Tyrannosaurus*, initially describing the otic joint as immobilized by the pterygoid, quadratojugal, and squamosal via sutures between the quadrate and surrounding bones. Osborn's description of the otic joint was refuted by Molnar (1991) who recognized that, although the otic joint was surrounded by sutured elements, the joint itself was smooth and saddle shaped which in turn led to subsequent functional analyses of otic joint kinesis by Molnar (1991, 1998), Rayfield (2005a), and Larsson (2008). Larsson (2008) supported inferences of propalinal (fore–aft) movement of the *Tyrannosaurus* palate, stating that movement was possible due to osteological anatomy, kinetically competent joints throughout the palate, and streptostylic movement of the quadrate. Molnar (1991, 1998) described streptostylic movement as well, stating that the otic joint could allow for "swings in several directions" (1991, p. 163) and was capable of resisting forces in multiple directions. Although streptostyly and propalinal palatal movements, as a result, appear reasonable in a disarticulated specimen, the rigidity of the facial skeleton, congruency of the otic joint, and the similarities between the neutral and FAM models suggest that any movement of the palate was incidental and potentially injurious to *Tyrannosaurus*. Moreover, the craniofacial skeleton of adult tyrannosaurs has numerous bony features that defy translational movements of the palate including the following: rigid, unbendable bones, a secondary palate built by massive, co-sutured maxillae, and heavily interdigitated sutural and scarf joints like the frontonasal, circummaxillary, and temporal joints (Carr, 1999; Snively et al., 2006). These lines of evidence all suggest *Tyrannosaurus* was functionally akinetic, despite possessing unsutured otic and palatobasal joints (Figs. 9 and 10).

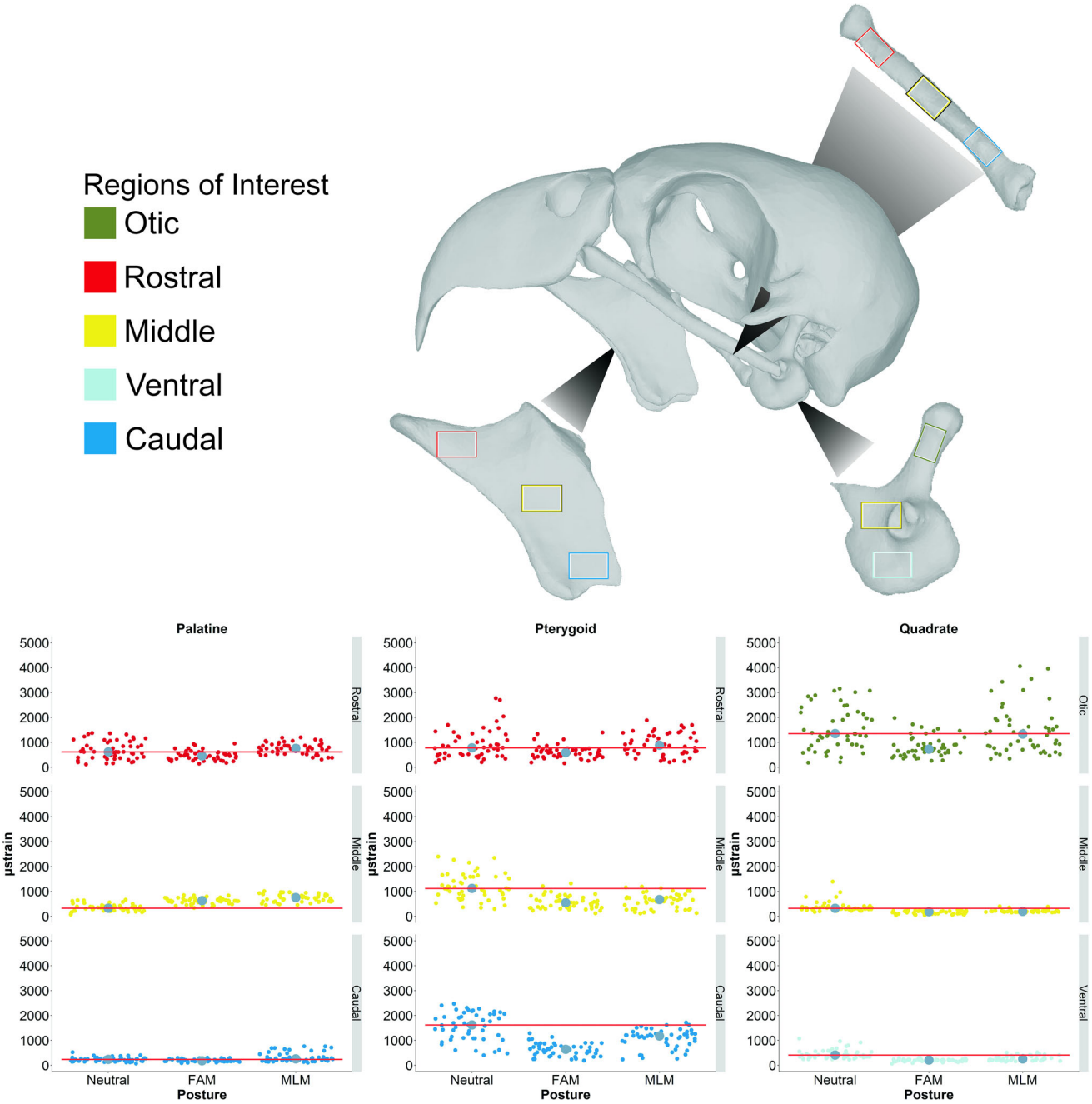

Fig. 7. Strains of regions of interest in the palatal elements of *Psittacus erithacus*. Regions of interest and scatter plots showing individual sample points as well as median strains (color-coded by sampling region) are represented. Otic, middle, and ventral regions correspond to sampling of the quadrate whereas Rostral, middle, and caudal regions correspond to sampling areas of the palatine and pterygoid. Each sampling region consists of 50 tetrahedra sampled randomly from the surface of the skeletal element. Horizontal lines representing the median value of the neutral posture are shown in red in each region of the palatal bones to facilitate comparison across postures.

Challenges to Modeling Kinesis and Cranial Function

Despite advances over previous modeling approaches, our process has several important sources of error and uncertainty, including tissue material properties, joint posture and range of motion, and jaw muscle activation patterns. We also acknowledge that taphonomic issues and reconstruction of fossils lead to potential sources of error in modeling extinct taxa as described by Hedrick et al. (2019). Material properties of non-osseous tissues are not well described outside of mammals and are unknown for large, extinct theropod dinosaurs. Wang et al. (2012;

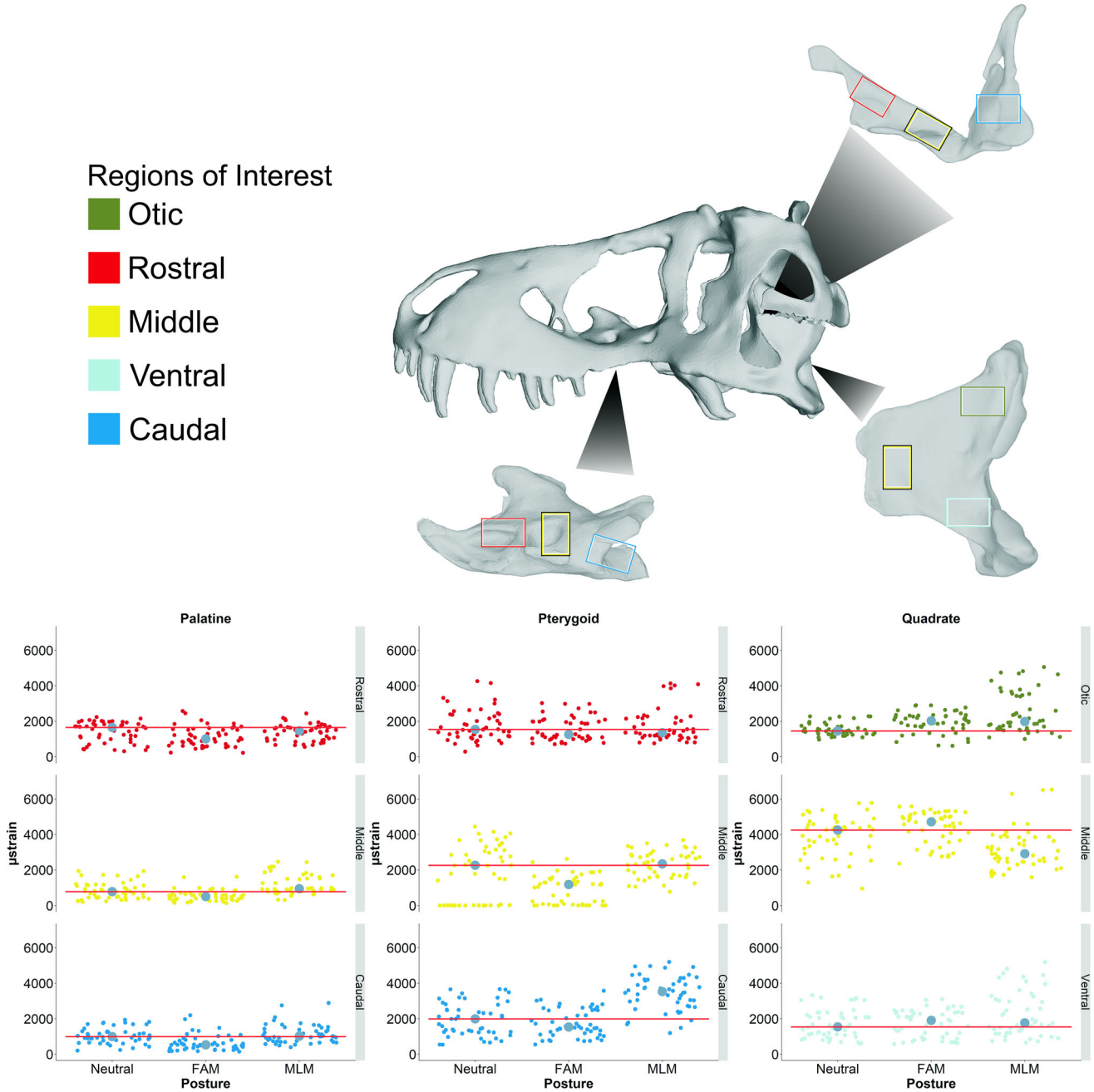

Fig. 8. Strains of regions of interest in the palatal elements of *Tyrannosaurus rex*. Regions of interest and scatter plots showing individual sample points as well as median strains (color-coded by sampling region) are represented. Otic, middle, and ventral regions correspond to sampling of the quadrate whereas Rostral, middle, and caudal regions correspond to sampling areas of the palatine and pterygoid. Each sampling region consists of 50 tetrahedra sampled randomly from the surface of the skeletal element. Horizontal lines representing the median value of the neutral posture are shown in red in each region of the palatal bones to facilitate comparison across postures.

testing of various material properties), Lautenschlager (2013; testing of beaks, teeth, and bone), and Cuff et al. (2015; validation study) all explored the impact of various material properties in mammal, dinosaur, and bird FEMs. We used these studies to inform our assignments of skeletal and articular properties to models, bearing in mind that Strait et al. (2005) noted that elastic properties have small impacts on model performance. We therefore constructed our joints with separate materials for the large cranium of *Tyrannosaurus* (canine patellar tendon) and the smaller crania of *Psittacus* and *Gekko* (rat cranial suture). Although sutural areas and joints were modeled in other studies (e.g., Moazen et al., 2009; Jones et al., 2011, 2017; Porro et al., 2011) as FEM elements assigned the properties of sutural or joint materials, this method retains a tightly packed area of the model which

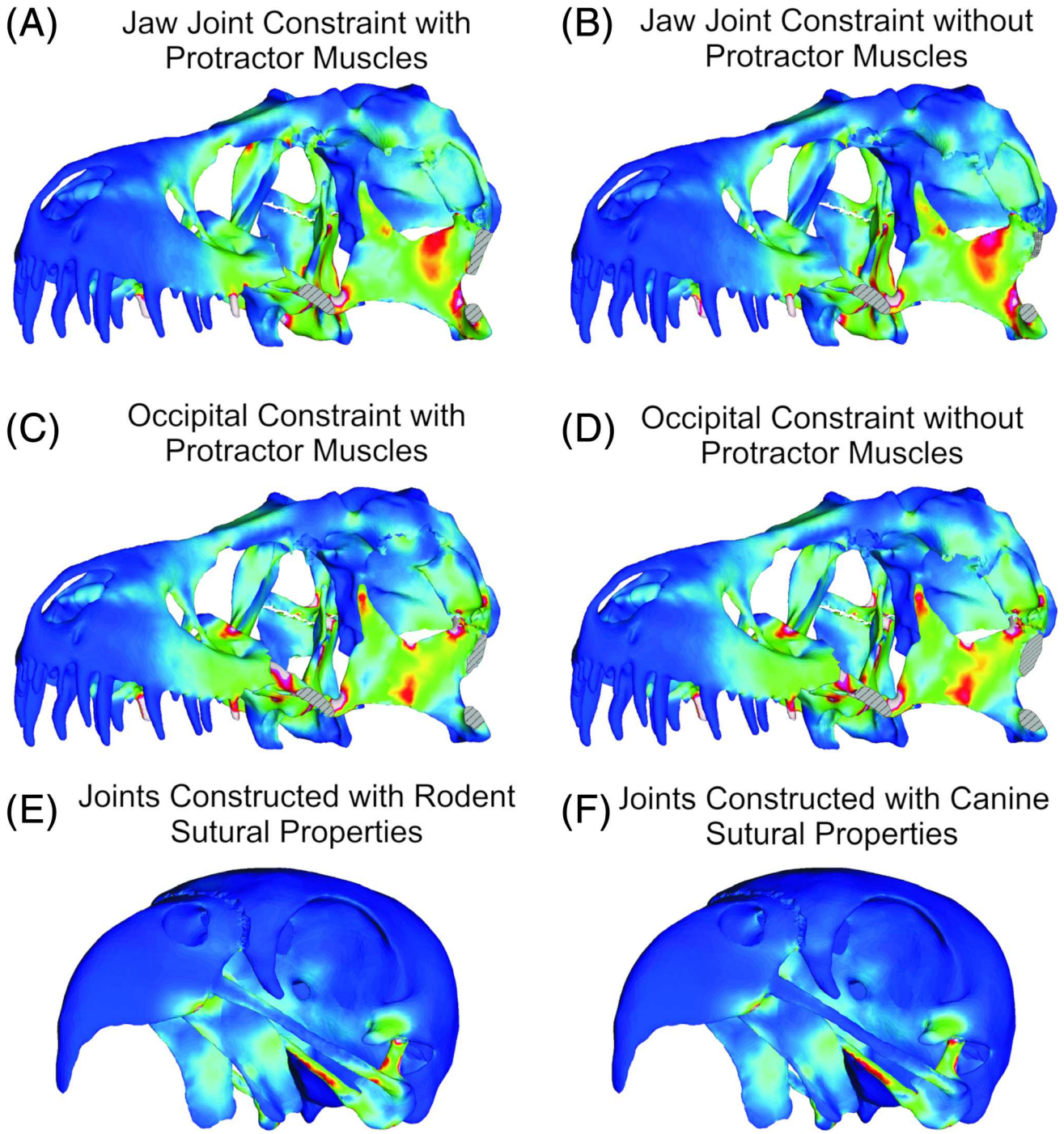

Fig. 9. Comparison of neutral postures of *Tyrannosaurus rex* and *Psittacus erithacus* in left rostrolateral view showing effects of protractor muscle activation, constraints, and sutural materials on the behavior of models. Jaw joint constraints with activated (**A**) and deactivated (**B**) protractor muscles reveal few differences in strains in the model. Occipital constraints with activated (**C**) and deactivated (**D**) protractor muscles reveal significant differences in strain distribution in the palate. Regions of models with hatching represent areas that have been cut away to allow for better visualizations of internal structures. *Psittacus erithacus* is presented to show differences between using rodent sutural properties (**E**) and canine sutural properties (**F**). Rodent sutural properties were used in *Psittacus* and *Gekko* and canine sutural properties were used in *Tyrannosaurus*. Sutural properties were considered based on taxon size.

would instead be occupied by more flexible material allowing for more deformation in sutures and joints involved in cranial kinesis; cranial sutures not associated with kinesis are less flexible. We consider our method of creating open spaces within the joint capsules of the model and joining these portions using flexible beams to more accurately simulate malleable soft tissue by permitting more realistic deformation at joints; however, further studies are needed

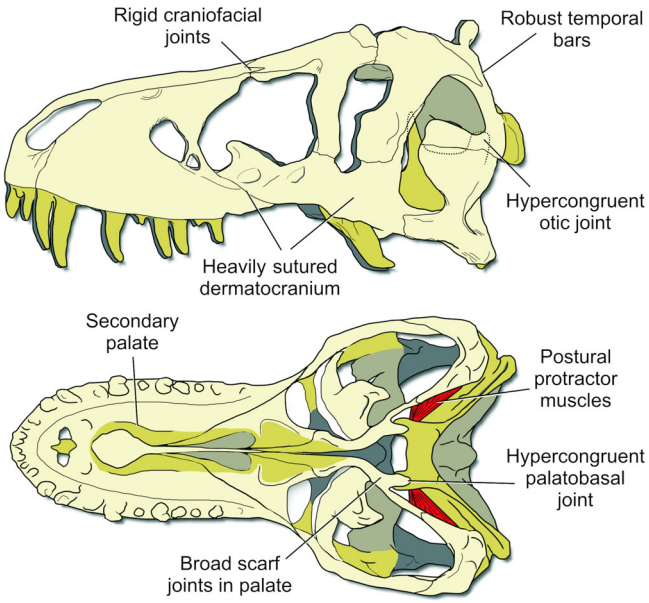

Fig. 10. Illustration of *Tyrannosaurus* skull in left lateral (top) and ventral (bottom) views with key functional characteristics of the feeding apparatus. Numerous features of the skull of *Tyrannosaurus* suggest it was not capable of substantial cranial kinesis.

to validate these findings. Node anomalies at joint articulations are a result of this joint construction, but do not change the overall strain patterns of the model with fused joints.

Static postures in our models are merely moments in a coordinated series of motions during feeding bouts. Although we only tested three specific instances of what could be a dynamically changing joint articulation, recent studies of ball and socket joints suggest that despite their seemingly flexible ranges of motion, they do not necessarily perform this way (e.g., Manafzadeh and Padian, 2018). Moazen et al. (2008) suggested that the temporal ligaments in *Uromastyx* stabilized the quadrate during feeding. Analogously, Manafzadeh and Padian (2018) found that only 10% of possible postures were valid once capsular ligaments were included in the ball and socket-shaped articulation. Indeed, *Tyrannosaurus* quadrates possess enlarged tuberosities on the medial portion of the otic process that bear the features of attachments for large capsular ligaments and complementary ligamentous scars adorn the lateral portion of the otic joint. Likewise, the palatobasal joint is highly congruent with a labrum of pterygoid bone nearly encompassing the basipterygoid condyle, further suggesting pronounced capsular ligaments. Thus, bony joint morphology (Holliday and Witmer, 2007), loading, and postural analysis suggest that a miniscule, and likely biologically insignificant, envelope of motion was available for the 6-bar linkage system of the robustly built *Tyrannosaurus* palate, which spans pairs of highly congruent palatobasal, otic, and craniofacial joints compared to the relatively freely moving bird hip joints. Finally, despite slight vagaries in the articulation of our model and that of the original BHI 3033 mount (e.g., palatobasal articulations, epipterygoid-pterygoid joint), these morphologies still likely fall within the possible natural variation of the *T. rex* population making our results biologically realistic and similar to other studies of posture and range of motion (e.g., Gatesy et al., 2010; Mallison, 2010; Claes et al., 2017; Olsen et al., 2017).

We modeled jaw muscles as contracting synchronously at maximal force even though it was likely that, as has been shown in other diapsids, there is variation in the firing sequence and magnitude of cranial musculature (Busbey, 1989; Nuijens et al., 1997; Herrel et al., 1999; van der Meij and Bout, 2008; Vinyard et al., 2008; Perry and Prufrock, 2018). Protractor and adductor muscles show variation in activation pattern during the feeding cycle, and the loads these muscles impart appear to help stabilize the cranial joints (Cundall, 1983; Herrel et al., 1999; Holliday and Witmer, 2007). Moreover, the orientation and osteological correlates of the m. protractor pterygoideus indicate that it was highly tendinous, likely pennate, and oriented dorsoventrally and mediolaterally (Holliday, 2009). This architecture suggests m. protractor pterygoideus had very limited excursion, and, at best, held the palate against the braincase, restraining its movements and filling a largely postural role.

Finally, to further understand the role of muscle loads and constraints on the model, we conducted *post hoc* tests with neutral *Tyrannosaurus* models using occipital constraints as well as differential activation of the protractor muscles. Constraints on the occipital surface of the skull were modeled to mimic cervical muscle loads imparted during inertial feeding mechanisms (Snively and Russell, 2007; Snively et al., 2014) as well as to free the jaw joint from artificial constraints. Additionally, protractor muscles were toggled on and off in the neutral *T. rex* model to test for their effect on palatal strains. Protractor muscles were found to not alter the distribution and range of strains in the palate suggesting they may not be functionally important, and even may be potentially vestigial. Conversely, occipital constraints shifted and diminished the strains experienced by the quadrate and pterygoid, but increased strains experienced by the epipterygoid as it was cantilevered by its laterosphenoid attachment. Regardless, the low strains experienced by the braincase in the neutral and FAM models in all tests indicate that although the palate was incapable of movement, it was capable of dissipating high strains away from the braincase, thus insulating the neurosensory capsules of the head (Holliday and Witmer, 2007).

CONCLUSIONS

This study presents a unique method of exploring *Tyrannosaurus* cranial kinesis that incorporates anatomically distinct, distributed muscle loadings, reconstructions of joint tissues, varying postures of cranial elements, and ultimately analysis of cranial performance using finite element modeling. Its new approaches differ from previous inferences of muscle architecture (Gignac and Erickson, 2017), joint function (Molnar, 1991; Rayfield, 2004, 2005a, b), and joint kinematics (Larsson, 2008). The findings presented here offer a nuanced, integrative approach to testing biomechanical hypotheses of cranial function in extant as well as extinct vertebrate species. Not only are these methods applicable to testing *a priori* assumptions about kinematics and function in living animals, but they also offer a detailed approach to testing behavioral and functional hypotheses in animals that are impossible to explore using *in vivo* approaches. Few modeling studies incorporate multiple lines of evidence, such as multiple postures, joint tissues, and distributed muscle loadings in such diverse species, and here we illustrate how

powerful these inferential approaches can be using *Tyrannosaurus* as a case study. These approaches found inferences of gross cranial mobility in *Tyrannosaurus* to be unsupported and that *Tyrannosaurus* was functionally akinetic.

ACKNOWLEDGEMENTS

We thank the University of Missouri Biomolecular Imaging Center and OhioHealth O'Bleness Hospital (Athens, Ohio) for scanning specimens. We thank Juliann Tea, Emily Rayfield, Anthony Herrel, Marc Jones, and Eric Snively for providing advice and assistance during the development of this study. We thank Peter Larson at the Black Hills Institute and Art Anderson at Virtual Surfaces for permission to use the 3D model of BHI 3033. We thank Emily Rayfield, Marc Jones, and Brandon Hedrick for comments that improved this manuscript's clarity and content. Finally, we thank Brandon Hedrick and Peter Dodson for inviting us to the special issue. Models are publically hosted on Open Science Framework: BirdNet: https://osf.io/e3v7u/.

LITERATURE CITED

Abdala V, Moro S. 1996. Cranial musculature of South American Gekkonidae. J Morphol 229:59–70.

Anderson RA, McBrayer LD, Herrel A. 2008. Bite force in vertebrates: opportunities and caveats for use of a nonpareil whole-animal performance measure. Biol J Linn Soc 93:709–720.

Bates KT, Falkingham PL. 2012. Estimating maximum bite performance in *Tyrannosaurus rex* using multi-body dynamics. Biol Lett 8:660–664.

Bates KT, Falkingham PL. 2018. The importance of muscle architecture in biomechanical reconstructions of extinct animals: a case study using *Tyrannosaurus rex*. J Anat 233:625–635.

Bock WJ. 1964. Kinetics of the avian skull. J Morphol 114:1–41.

Bock WJ. 1999. Cranial kinesis revisited. Zool Anz 238:27–39.

Bout RG, Zweers GA. 2001. The role of cranial kinesis in birds. Comp Biochem Physiol A Mol Integr Physiol 131:197–205.

Burton PJK. 1974a. Jaw and tongue features in Psittaciformes and other orders with special reference to the anatomy of the Toothbilled pigeon (*Didunculus strigirostris*). J Zool 174:255–276.

Burton PJK. 1974b. *Feeding and the feeding apparatus in waders: a study of anatomy and adaptations in the Charadrii*, Vol. 719. London: British Museum (National History). p 1–150.

Busbey AB. 1989. Form and function of the feeding apparatus of *Alligator mississippiensis*. J Morphol 202:99–127.

Campbell AM, Cler ML, Skurla CP, Kuehl JJ. 2016. Damage accumulation of bovine bone under variable amplitude loads. Bone Rep 5:320–332.

Carr TD. 1999. Craniofacial ontogeny in Tyrannosauridae (Dinosauria, Coelurosauria). J Vertebr Paleontol 19:497–520.

Carril J, Degrange FJ, Tambussi CP. 2015. Jaw myology and bite force of the monk parakeet (Aves, Psittaciformes). J Anat 227: 34–44.

Chien CH, Wu YD, Chao YJ, Chen T, Chen WF, Yu JC, Li X. 2008. The effects of different cranial modules on mechanical properties of cranial suture in Lewis rats and same-–aged C57BL/6 mice. Strain 44:272–277.

Claes R, Muyshondt PGG, Van Hoorebeke L, Dhaene J, Dirckx JJJ, Aerts P. 2017. The effect of craniokinesis on the middle ear of domestic chickens (*Gallus gallus domesticus*). J Anat 230:414–423.

Cuff AR, Bright JA, Rayfield EJ. 2015. Validation experiments on finite element models of an ostrich (*Struthio camelus*) cranium. PeerJ 3:e1294.

Cundall D. 1983. Activity of head muscles during feeding by snakes: a comparative study. Am Zool 23:383–396.

Curtis N, Jones MEH, Evans SE, O'Higgins P, Fagan MJ. 2010. Feedback control from the jaw joints during biting: an investigation of the reptile *Sphenodon* using multibody modelling. J Biomech 43: 3132–3137.

Curtis N, Jones MEH, Shi J, O'Higgins P, Evans SE, Fagan MJ. 2011. Functional relationship between skull form and feeding mechanics in *Sphenodon*, and implications for diapsid skull development. PLoS One 6:e29804.

Curtis N, Jones MEH, Evans SE, O'Higgins P, Fagan MJ. 2013. Cranial sutures work collectively to distribute strain throughout the reptile skull. J R Soc Interface 10:1–9.

Davis JL, Santana SE, Dumont ER, Grosse IR. 2010. Predicting bite force in mammals: two-dimensional versus three-dimensional lever models. J Exp Biol 213:1844–1851.

Dawson MM, Metzger KA, Baier DB, Brainerd EL. 2011. Kinematics of the quadrate bone during feeding in mallard ducks. J Exp Biol 214:2036–2046.

Daza JD, Mapps AA, Lewis PJ, Thies ML, Bauer AM. 2015. Peramorphic traits in the tokay gecko skull. J Morphol 276: 915–928.

Erickson GM, Lappin AK, Vliet KA. 2003. The ontogeny of bite-force performance in American alligator (*Alligator mississippiensis*). J Zool 260:317–327.

Evans SE. 2003. At the feet of the dinosaurs: the early history and radiation of lizards. Biol Rev Camb Philos Soc 78:513–551.

Frost HM. 1987. Bone "mass" and the "mechanostat": a proposal. Anat Rec 210:1–9.

Gans C, De Vree F. 1987. Functional bases of fiber length and angulation in muscle. J Morphol 192:63–85.

Gatesy SM, Bäker M, Hutchinson JR. 2010. Constraint-based exclusion of limb poses for reconstructing theropod dinosaur locomotion. J Vertebr Paleontol 29:535–544.

Gignac PM, Erickson GM. 2017. The biomechanics behind extreme osteophagy in *Tyrannosaurus rex*. Sci Rep 7:2012.

Grosse IR, Dumont ER, Coletta C, Tolleson A. 2007. Techniques for modeling muscle-induced forces in finite element models of skeletal structures. Anat Rec 290:1069–1088.

Gussekloo SWS. 2000. *The evolution of the Paleognathous birds: functional morphology and evolutionary patterns*. Leiden: Leiden University.

Gussekloo SWS. 2005. Cranial kinesis in palaeognathous birds. J Exp Biol 208:3409–3419.

Haas G. 1973. Muscles of the jaws and associated structures in the Rhynchocephalia and Squamata. In: Gans C, Parsons T, editors. *Biology of the reptilia*, Vol. 4. London: Academic Press. p 285–483.

Haut RC, Lancaster RL, DeCamp CE. 1992. Mechanical properties of the canine patellar tendon: some correlations with age and the content of collagen. J Biomech 25:163–173.

Hedrick BP, Schachner ER, Rivera G, Dodson P, Pierce SE. 2019. The effects of skeletal asymmetry on interpreting biologic variation and taphonomy in the fossil record. Paleobiology 45: 154–166.

Herrel A, De Vree F, Delheusy V, Gans C. 1999. Cranial kinesis in gekkonid lizards. J Exp Biol 202:3687–3698.

Herrel A, Aerts P, De Vree F. 2000. Cranial kinesis in geckoes: functional implications. J Exp Biol 203:1415–1423.

Herrel A, Schaerlaeken V, Meyers JJ, Metzger KA, Ross CF. 2007. The evolution of cranial design and performance in squamates: consequences of skull-bone reduction on feeding behavior. Integr Comp Biol 47:107–117.

Herring SW, Ochareon P. 2005. Bone—special problems of the craniofacial region. Orthod Craniofac Res 8:174–182.

Hieronymus TL. 2006. Quantitative microanatomy of jaw muscle attachment in extant diapsids. J Morphol 267:954–967.

Hoese WJ, Westneat MW. 1996. Biomechanics of cranial kinesis in birds: testing linkage models in the white-throated sparrow (*Zonotrichia albicollis*). J Morphol 227:305–320.

Hofer H. 1949. Die Gaumenlucken der Vogel. Acta Zool 30: 210–248.

Hofer H. 1950. Zur Morphologie der Kiefermuskulatur der Vögel. Zool Jahrb Abt Anat Ontogenie Tiere 70:427–556.

Holliday CM. 2009. New insights into dinosaur jaw muscle anatomy. Anat Rec 292:1246–1265.

Holliday CM, Witmer LM. 2007. Cranial kinesis in dinosaurs: intracranial joints, protractor muscles, and their significance for cranial evolution and function in diapsids. J Vertebr Paleontol 28: 1073–1088.

Holliday CM, Witmer LM. 2009. The epipterygoid of crocodyliforms and its significance for the evolution of the orbitotemporal region of eusuchians. J Vert Paleontol 29:715–733.

Jones MEH, Curtis N, Fagan MJ, O'Higgins P, Evans SE. 2011. Hard tissue anatomy of the cranial joints in *Sphenodon* (Rhynchocephalia): sutures, kinesis, and skull mechanics. Palaeontol Electron 14:1–56.

Jones MEH, Groning F, Dutel H, Sharp A, Fagan MJ, Evans SE. 2017. The biomechanical role of the chondrocranium and sutures in a lizard cranium. J R Soc Interface 14:20170637.

Larsson HCE. 2008. Palatal kinesis of *Tyrannosaurus rex*. In: Larson PL, Carpenter K, editors. Tyrannosaurus rex*, the tyrant king*. Bloomington: University of Indiana Press. p 245–252.

Lautenschlager S. 2013. Cranial myology and bite force performance of Erlikosaurus andrewsi: a novel approach for digital muscle reconstructions. J Anat 222:260–272.

Lautenschlager S. 2015. Estimating cranial musculoskeletal constraints in theropod dinosaurs. R Soc Open Sci 2:1–14.

Lautenschlager S, Witmer LM, Altangerel P, Rayfield EJ. 2013. Edentulism, beaks, and biomechanical innovations in the evolution of theropod dinosaurs. Proc Natl Acad Sci USA 110: 20657–20662.

Mallison H. 2010. CAD assessment of the posture and range of motion of *Kentrosaurus aethiopicus* Hennig 1915. Swiss J Geosci 103:211–233.

Manafzadeh AR, Padian K. 2018. ROM mapping of ligamentous constraints on avian hip mobility: implications for extinct ornithodirans. Proc R Soc B Biol Sci 285:1–9.

Martin RB. 2000. Toward a unifying theory of bone remodeling. Bone 26:1–6.

van der Meij MAA, Bout RG. 2008. The relationship between shape of the skull and bite force in finches. J Exp Biol 211:1668–1680.

Metzger K. 2002. Cranial kinesis in lepidosaurs: skulls in motion. In: Aerts P, D'Aout K, Herrel A, Van Damme R, editors. *Topics in functional and ecological vertebrate morphology*. Maastricht: Shaker Publishing B. V. p 15–46.

Mezzasalma M, Maio N, Guarino FM. 2014. To move or not to move: cranial joints in European gekkotans and lacertids, an osteological and histological perspective. Anat Rec 297:463–472.

Moazen M, Curtis N, Evans SE, O'Higgins P, Fagan MJ. 2008. Combined finite element and multibody dynamics analysis of biting in a *Uromastyx hardwickii* lizard skull. J Anat 213: 499–508.

Moazen M, Curtis N, O'Higgins P, Jones MEH, Evans SE, Fagan MJ. 2009. Assessment of the role of sutures in a lizard skull: a computer modelling study. Proc R Soc B Biol Sci 276:39–46.

Molnar RE. 1991. The cranial morphology of *Tyrannosaurus rex*. Palaeontogr Abt A 217:137–176.

Molnar RE. 1998. Mechanical factors in the design of the skull of *Tyrannosaurus rex* (Osborn, 1905). Gaia Ecol Perspect Sci Soc 15: 193–218.

Molnar RE. 2008. Reconstruction of the jaw musculature of *Tyrannosaurus rex*. In: Larson PL, Carpenter K, editors. Tyrannosaurus rex*, the tyrant king*. Bloomington: Indiana University Press. p 254–281.

Montuelle SJ, Williams SH. 2015. In vivo measurement of mesokinesis in *Gekko gecko*: the role of cranial kinesis during gape display, feeding and biting. PLoS One 10:e0134710.

Nuijens FW, Snelderwaard PC, Bout RG. 1997. An electromyographic technique for small animals. J Neurosci Methods 76:71–73.

Olsen AM, Camp AL, Brainerd EL. 2017. The opercular mouthopening mechanism of largemouth bass functions as a 3D four-bar linkage with three degrees of freedom. J Exp Biol 220:4612–4623.

Osborn HF. 1912. Crania of *Tyrannosaurus* and *Allosaurus*. Mem Am Museum Nat Hist 1:1–32.

Payne SL, Holliday CM, Vickaryous MK. 2011. An osteological and histological investigation of cranial joints in geckos. Anat Rec 294: 399–405.

Perry JM, Prufrock KA. 2018. Muscle functional morphology in paleobiology: the past, present, and future of "Paleomyology". Anat Rec 301:538–555.

Pol D, Rauhut OWM, Lecuona A, Leardi JM, Xu X, Clark JM. 2013. A new fossil from the Jurassic of Patagonia reveals the early basicranial evolution and the origins of Crocodyliformes. Biol Rev Camb Philos Soc 88:862–872.

Porro LB, Holliday CM, Anapol F, Ontiveros LC, Ontiveros LT, Ross CF. 2011. Free body analysis, beam mechanics, and finite element modeling of the mandible of *Alligator mississippiensis*. J Morphol 272:910–937.

Rayfield EJ. 2004. Cranial mechanics and feeding in *Tyrannosaurus rex*. Proc R Soc B Biol Sci 271:1451–1459.

Rayfield EJ. 2005a. Using finite-element analysis to investigate suture morphology: a case study using large carnivorous dinosaurs. Anat Rec Part A Discov Mol Cell Evol Biol 283A: 349–365.

Rayfield EJ. 2005b. Aspects of comparative cranial mechanics in the theropod dinosaurs Coelophysis, Allosaurus and Tyrannosaurus. Zool J Linn Soc 144:309–316.

Rayfield EJ. 2011. Strain in the ostrich mandible during simulated pecking and validation of specimen-specific finite element models. J Anat 218:47–58.

Reed DA, Porro LB, Iriarte-Diaz J, Lemberg JB, Holliday CM, Anapol F, Ross CF. 2011. The impact of bone and suture material properties on mandibular function in *Alligator mississippiensis*: testing theoretical phenotypes with finite element analysis. J Anat 218:59–74.

Reilly GC, Currey JD. 1999. The development of microcracking and failure in bone depends on the loading mode to which it is adapted. J Exp Biol 202:543–552.

Rieppel OC. 1978. The phylogeny of cranial kinesis in lower vertebrates, with special reference to the Lacertilia. N Jb Geol Palaont Abh 156:353–370.

Rieppel OC. 1984. The structure of the skull and jaw adductor musculature in the Gekkota, with comments on the phylogenetic relationships of the Xantusiidae (Reptilia:Lacertilia). Zool J Linn Soc 82:291–318.

Sacks RD, Roy RR. 1982. Architecture of the hind limb muscles of cats: functional significance. J Morphol 173:185–195.

Sellers KC, Middleton KM, Davis JL, Holliday CM. 2017. Ontogeny of bite force in a validated biomechanical model of the American alligator. J Exp Biol 220:2036–2046.

Smith KK, Hylander WL. 1985. Strain gauge measurement of mesokinetic movement in the lizard *Varanus exanthematicus*. J Exp Biol 114:53–70.

Snively E, Russell AP. 2007. Functional morphology of neck musculature in the Tyrannosauridae (Dinosauria, Theropoda) as determined via a hierarchical inferential approach. Zool J Linn Soc 151: 759–808.

Snively E, Henderson DM, Phillips DS. 2006. Fused and vaulted nasals of tyrannosaurid dinosaurs: implications for cranial strength and feeding mechanics. Acta Palaeontol Pol 51: 435–454.

Snively E, Russell AP, Powell GL, Theodor JM, Ryan MJ. 2014. The role of the neck in the feeding behaviour of the Tyrannosauridae: inference based on kinematics and muscle function of extant avians. J Zool 292:290–303.

Strait DS, Wang Q, Dechow PC, Ross CF, Richmond BG, Spencer MA, Patel BA. 2005. Modeling elastic properties in finite-element analysis: how much precision is needed to produce an accurate model? Anat Rec Part A Discov Mol Cell Evol Biol 283A: 275–287.

Tokita M. 2003. The skull development of parrots with special reference to the emergence of a morphologically unique cranio-facial hinge. Zool Sci 20:749–758.

Tokita M. 2004. Morphogenesis of parrot jaw muscles: understanding the development of an evolutionary novelty. J Morphol 259:69–81.

Tseng ZJ, Binder WJ. 2010. Mandibular biomechanics of *Crocuta crocuta*, *Canis lupus*, and the late Miocene *Dinocrocuta gigantea* (Carnivora, Mammalia). Zool J Linn Soc 158:683–696.

Versluys J. 1910. Streptostylie bei Dinosaurien, nebst Bemerkungen uber die verwandtschaft der vogel und Dinosaurier. Zool Jahrb Abt Anat Ontogenie Tiere 30:175–260.

Vinyard CJ, Wall CE, Williams SH, Hylander WL. 2008. Patterns of variation across primates in jaw-muscle electromyography during mastication. Integr Comp Biol 48:294–311.

Wang Q, Wood SA, Grosse IR, Ross CF, Zapata U, Byron CD, Wright SA, Strait DS. 2012. The role of the sutures in biomechanical dynamic simulation of a macaque cranial finite element model: implications for the evolution of craniofacial form. Anat Rec 295: 278–288.

Wroe S, McHenry C, Thomason J. 2005. Bite club: comparative bite force in big biting mammals and the prediction of predatory behaviour in fossil taxa. Proc R Soc B Biol Sci 272:619–625.

Zusi RL. 1967. The role of the depressor mandibulae muscle in kinesis of the avian skull. Proc U S Natl Mus 123:1–28.

Zusi RL. 1984. A functional and evolutionary analysis of rhynchokinesis in birds. Smithson Contrib Zool 395:1–40.

Zusi RL. 1993. Patterns of diversity in the avian skull. In: Hanken J, Hall BK, editors. *The skull 2: patterns of structural and systematic diversity*. Chicago: The University of Chicago Press. p 391–437.